Environmental Science: Atmospheres

ROYAL SOCIETY OF CHEMISTRY

PAPER

View Article Online
View Journal | View Issue

Cite this: *Environ. Sci.: Atmos.*, 2023, **3**, 581

Wildfire particulate matter as a source of environmentally persistent free radicals and reactive oxygen species†

Ting Fang, Brian C. H. Hwang, Sukriti Kapur, Katherine S. Hopstock, Jinlai Wei, Vy Nguyen, Sergey A. Nizkorodov and Manabu Shiraiwa *

Wildfires, which have been occurring increasingly in the era of climate change, emit massive amounts of particulate matter (PM) into the atmosphere, strongly affecting air quality and public health. Biomass burning aerosols may contain environmentally persistent free radicals (EPFRs, such as semiquinone radicals) and redox-active compounds that can generate reactive oxygen species (ROS, including ·OH, superoxide and organic radicals) in the aqueous phase. However, there is a lack of data on EPFRs and ROS associated with size-segregated wildfire PM, which limits our understanding of their climate and health impacts. We collected size-segregated ambient PM in Southern California during two wildfire events to measure EPFRs and ROS using electron paramagnetic resonance spectroscopy. EPFRs are likely associated with soot particles as they are predominantly observed in submicron particles (PM_1, aerodynamic diameter ≤ 1 μm). Upon extraction in water, wildfire PM mainly generates ·OH (28–49%) and carbon-centered radicals (~50%) with minor contributions from superoxide and oxygen-centered organic radicals (2–15%). Oxidative potential measured with the dithiothreitol assay (OP-DTT) is found to be high in wildfire PM_1, exhibiting little correlation with the radical forms of ROS (r^2 ≤ 0.02). These results are in stark contrast with PM collected at highway and urban sites, which generates predominantly ·OH (84–88%) that correlates well with OP-DTT (r^2 ~ 0.6). We also found that PM generated by flaming combustion generates more radicals with higher OP-DTT compared to those by smoldering or pyrolysis.

Received 2nd December 2022
Accepted 27th January 2023

DOI: 10.1039/d2ea00170e

rsc.li/esatmospheres

Environmental significance

Environmentally persistent free radicals (EPFRs) and reactive oxygen species (ROS) are increasingly recognized for adverse health impacts of ambient particulate matter (PM). However, these reactive species are poorly characterized in PM emitted from wildfires. This study has investigated the occurrence of EPFRs and ROS generation in particles of different sizes from two wildfire events in Southern California, and found that wildfires are significant sources of EPFRs contained in submicron particles. In addition, wildfire PM mainly spontaneously generates OH and carbon-centered radicals upon dissolution into water. The generated radicals exhibit little correlations with oxidative potential measured with the dithiothreitol assay that is hypothesized to represent toxicity. We stress the importance of characterizing free radicals for evaluating the impacts of wildfire PM on air quality and public health.

Introduction

Wildfires become more frequent in semiarid regions around the globe, posing large impacts on the atmosphere and ecosystems.[1,2] Wildfire activities have been intensifying in the Western United States.[3] Wildfires emit massive amounts of gaseous compounds and particulate matter (PM), strongly impacting outdoor and indoor air quality, climate, and human health.[4–9] Epidemiological studies have found that exposure to wildfire and biomass burning can cause cardiorespiratory illnesses[10,11] and exacerbate asthma,[12] and amplify COVID-19 cases and death.[13] As global warming and climate change progress, the occurrence and intensity of wildfires are projected to increase in the forthcoming century.[5,14]

Reactive oxygen species (ROS) play a central role in chemical transformation of atmospheric aerosols and adverse aerosol health effects by causing oxidative stress.[15–19] Wildfires release large amounts of particles composed of ash,[20,21] elemental carbon,[22] humic-like substance (HULIS),[23,24] polycyclic aromatic hydrocarbons (PAHs) and their derivatives,[25] and transition metals.[20] Some of these compounds are reactive and redox active, triggering the formation of ROS in the aqueous phase. For example, previous studies have shown that the

Department of Chemistry, University of California, Irvine, CA 92697-2025, USA. E-mail: m.shiraiwa@uci.edu

† Electronic supplementary information (ESI) available: Tables S1 and S2 and Fig. S1–S4. See DOI: https://doi.org/10.1039/d2ea00170e

decomposition of organic hydroperoxides and redox cycling of quinones can lead to the generation of ROS including hydroxyl (·OH), superoxide or hydroperoxyl ($\cdot O_2^-/\cdot HO_2$), and organic radicals.[26–28] Transition metals such as iron (Fe) and copper (Cu) can facilitate the formation of ·OH and organic radicals through Fenton-like reactions of peroxides and peracids,[29–31] which can be enhanced by photoirradiation for a rapid burst of ·OH production.[32] It has been reported that HULIS can enhance Fe-mediated reduction of oxygen to $\cdot O_2^-$ and destruction of H_2O_2 to form ·OH.[33] These condensed-phase generated oxidants can drive aqueous-phase chemistry in deliquesced particles and cloud/fog droplets, affecting their climatic effects such as optical properties and cloud condensation nuclei activity.[34]

PM oxidative potential (OP), often measured with the dithiothreitol (DTT) assay, has been suggested as an alternative indicator for aerosol toxicity beyond PM mass concentration. The underlying assumption is that the DTT decay rate would correspond to the rate of ROS formation.[35–37] Biomass burning is one of the major sources of OP-DTT in Europe, Asia, and the United States especially in winter seasons.[38–41] Redox-active species such as quinones,[42–44] HULIS,[45,46] and transition metals[47,48] and their complexes with organics[49–51] may contribute to OP-DTT. The relationship among toxicity, OP, and ROS formation by biomass burning PM still needs to be evaluated.

Combustion-derived particles contain stable radicals, so-called environmentally persistent free radicals (EPFRs).[52–55] EPFRs are found to remain stable with long lifetimes for days, months, and even indefinite, making them highly susceptible to long-range transport.[52,53,56] The chemical identities of EPFRs include semiquinone, phenoxyl, and cyclopentadienyl radicals. EPFRs may be directly released from incomplete combustion[57,58] or formed secondarily from chemical processing of PAHs in the atmosphere.[59] Ambient PM collected during bush fires as well as charcoal or burnt biomass was found to contain high concentrations of EPFRs.[7,53] A recent study showed that the emission factors of EPFRs in $PM_{2.5}$ from biomass burning were significantly higher than those from coal combustion.[60] EPFRs are redox active to reduce oxygen and sustain the generation of ROS including ·OH through quinoid redox cycling;[61–63] consequently, EPFRs may be cytotoxic to cause cell death.[64]

Wildfire PM is still poorly characterized with limited quantification regarding EPFRs, ROS formation, and OP; especially the size distribution of these properties has not been reported. The particle size is important for evaluating health impacts in different regions of the lung, as submicron particles can reach deep into the lung to the alveoli, while coarse particles would mostly deposit on upper airways.[65] In this study, we collected size-segregated ambient PM during two wildfire events in Irvine, California in 2020. EPFRs and ROS formation were quantified using a continuous-wave electron paramagnetic resonance (CW-EPR) spectrometer. EPFRs were measured by non-destructive direct analysis of the PM filter in EPR. ROS formation upon PM extraction in water was quantified using EPR combined with a spin-trapping technique. OP was measured by the DTT assay. The size distributions of EPFRs, ROS formation, and OP-DTT from wildfires are compared to those from ambient PM collected in highway and urban background environments. As the effects of burning conditions (combustion, smoldering, and pyrolysis) on PM oxidative potential and ROS formation are poorly understood, we also generated particles by combustion and pyrolysis in a laboratory for measurements of EPFRs, ROS, and OP-DTT.

Methods

PM collection

A Micro-Orifice Uniform Deposition Impactor (MOUDI, Model 100NR) was used to collect size-segregated ambient PM on Teflon filters (Millipore Omnipore Membrane Filter, PTFE, 0.2 μm pore size, JFWP04700) at an urban site, which is located on the rooftop of a campus building at the University of California, Irvine (UCI) (33°38′40.4″N 117°50′39.3″W, elevation 20 m). In winter 2020, two wildfire events occurred near the sampling site according to the California Department of Forestry and Fire Protection (CAL FIRE): Silverado and Bond Fires. The Silverado Fire started in Silverado Canyon (33°44′10.1″N 117°39′25.9″W) on October 26, 2020 and was contained on November 7, 2020. The Bond Fire was active around the California State Route 241 in the Irvine area (33°44′37.8″N 117°40′29.9″W) during December 2–10, 2020. These wildfire events were characterized with greatly reduced visibilities and substantial increases of PM mass concentrations up to 280 and 450 μg m^{-3} for submicron (PM_1) and coarse (PM_{10}) fractions, respectively (Fig. S1†). Fig. 1A shows the sampling sites and wildfire locations with the smoke plumes from the Silverado Fire on October 26, 2020 affecting the Irvine area. The fire location was roughly 20 km from the urban sampling site. We also collected ambient PM at two highway sites, which were approximately 2 m from the highway Interstate 5 (33°49′09.4″N 117°55′07.5″W) in Anaheim and 20 meters from Interstate 710 (33°51′34.0″N 118°12′01.0″W) in Long Beach.

Eight sets of MOUDI filter samples were collected at the urban location continuously for 3 days for each set during wildfire events from October 26 to December 9, 2020. Three MOUDI sets were collected at the highway sites (12 h on January 31, 2020 at the Anaheim site and 12 h on February 7, 2020 and 5.5 h on February 8, 2020 at the Long Beach site). Three sets were collected for 10–12 h daily at the urban site between February 23–25, 2020, which are considered as urban background samples. The detailed sampling dates and times are provided in Table S1.† The MOUDI was operated with selected stages with the remaining stages removed and without a backup filter at a flow rate of 30 L min^{-1}. The 50% cut-off aerodynamic diameters used for wildfire samples were 18, 10, 1, 0.18, and 0.056 μm, and those for the highway and urban samples were 18, 10, 3.2, 1, 0.56, and 0.056 μm, respectively. EPFRs, ROS formation, and OP-DTT in PM_1 and $PM_{1–10}$ are sums of the MOUDI stages up to 1 μm and between 1 and 10 μm, respectively. Field blanks were collected without turning on the MOUDI pump at each site ($N = 11$). After each collection, all blank and sample filters were stored in Petri dishes and immediately stored in a freezer (−18 °C). EPFRs, ROS

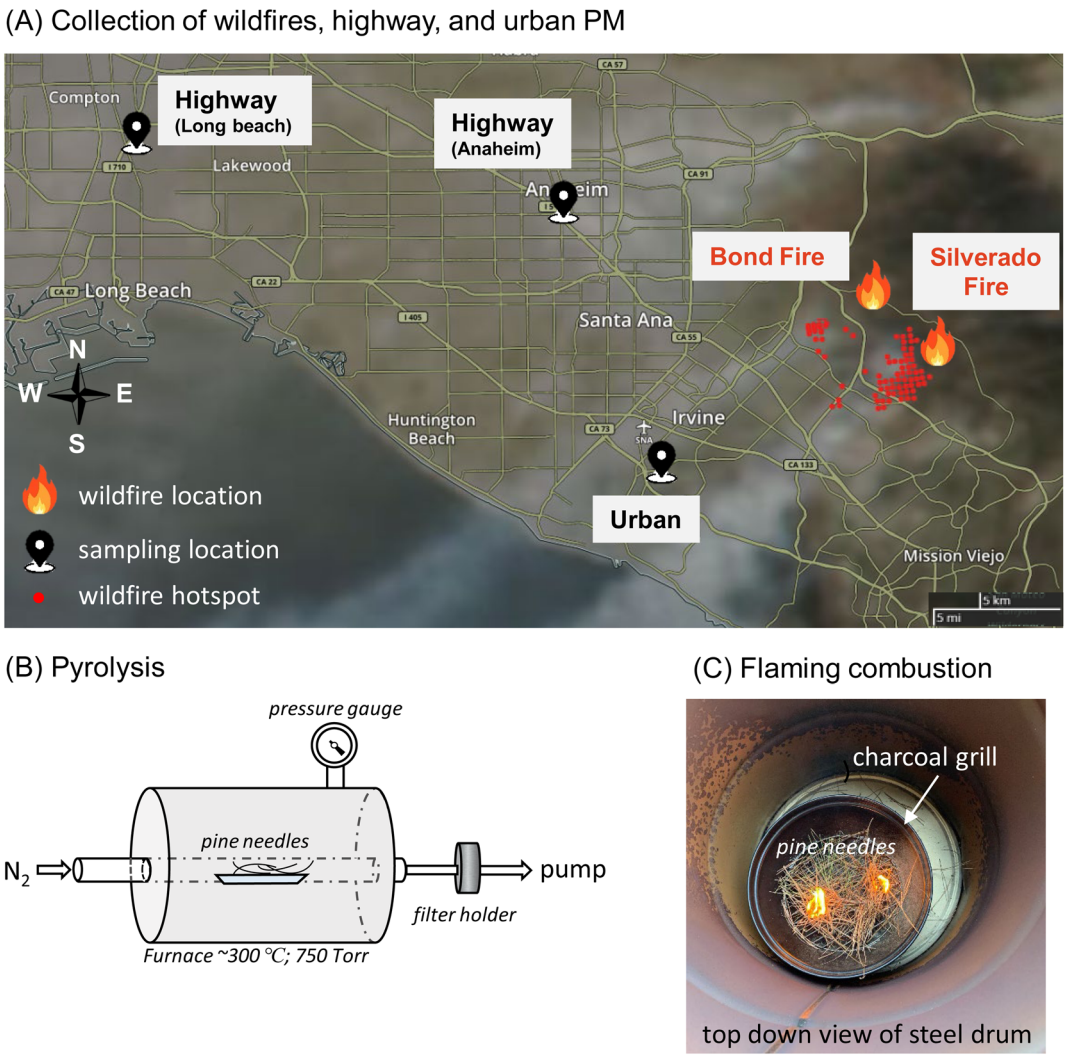

Fig. 1 (A) Sampling and wildfire locations, and the smoke plumes and wildfire hotspots from the Silverado Fire (on October 26, 2020) as viewed by the Moderate Resolution Imaging Spectroradiometer (MODIS). Laboratory combustion experiments with (B) pyrolysis and (C) flaming combustion of pine needles.

formation, and OP-DTT measurements were performed on these filter and blank samples following the procedures in our previous study.[52] EPFR measurements were conducted within 8 months of sample collection and ROS and DTT measurements were conducted within 8–18 months. Gehling and Dellinger (2013)[56] showed that a semiquinones-type radical has a half-life of 208 to 417 days and Sigmund *et al.* (2021)[53] revealed that EPFRs in wildfire charcoals can remain stable for years. In our previous work, we found that EPFRs in $PM_{2.5}$ samples collected at the same highway sites are stable at least a year after collection.[52] Some fraction of EPFRs are reported to have a shorter lifetime with days at room temperature,[56] so the EPFRs measured in this study likely do not include those with fast decay; hence, the reported EPFR concentrations in this study should be regarded as a lower limit. ROS and DTT measurements should not be impacted significantly by the filter storage, as the generation of ROS or the reaction with DTT occurs only upon filter extraction of stable PM compounds, respectively. The data are presented as per the volume of air sampled (pmol m^{-3} for EPFRv and ROSv, or nmol min^{-1} m^{-3} for total OP-DTTv) or per the mass of PM (pmol μg^{-1} for EPFRm and ROSm, or nmol min^{-1} μg^{-1} for OP-DTTm). The frequency size distributions of EPFRs, ROS formation, and OP were calculated by dividing the size distribution with the sum of activities from all MOUDI stages. Note that frequency distributions are independent of ambient levels which can vary substantially among different sites and sampling times. It should also be noted that dilution and chemical aging must have occurred upon transport of the plumes to the sampling site, affecting the chemical composition of primary-emitted biomass burning aerosols and forming secondary aerosols.[66,67] Therefore, our measurements should reflect the properties of both primary and secondary biomass burning aerosols.

PM mass concentrations

The hourly mass concentrations of PM_1 and PM_{10} for the urban site were obtained from the purple air real-time air quality data

from sensors located within 0.5 km from the sampling location (Aldrich Hall for urban and Multipurpose Science and Technology Building (MSTB) for wildfire samples). The mass concentration of PM_{1-10} was obtained by subtracting the mass concentration of PM_1 from PM_{10}. The PM mass concentrations during sampling periods were integrated and used to normalize the data of EPFRs, ROS, and total OP-DTT. Note that particles smaller than 56 nm were not collected, but they only represent a minor fraction of the mass. The Purple Air data were not available at the highway sites.

Environmentally persistent free radicals (EPFRs)

Each filter sample was folded and inserted into a quartz tube with an inner diameter of 9.17 mm and loaded into a resonator of a CW-EPR (EMXplus, Bruker) for measurements of EPFRs. The following EPR parameters were used for EPFR measurements: a microwave frequency of 9.65 GHz; a microwave power of 20 or 31.70 mW (microwave attenuation 8 or 10 dB); a modulation frequency of 100 kHz; a modulation amplitude of 3 G; a receiver gain of 40 dB; a time constant of 10.24 ms; a magnetic field scan of 1623 G. EPR measurement on the same sample was repeated for metal measurements with the same parameters except a larger magnetic field scan of 5600.4 G and a smaller time constant of 2.56 ms. The area of the EPR spectrum was integrated using Xenon software and converted to the total number of spins based on a calibration using standard 4-hydroxy-2,2,6,6-tetramethylpiperidinyloxy (TEMPOL) solutions ($N = 10$, $r^2 = 0.9999$, Fig. S2†).

Reactive oxygen species (ROS) formation

EPR combined with a spin-trapping technique was applied to measure the formation of ROS in the aqueous extracts of MOUDI samples. Half of each filter sample was vortexed for 8–10 minutes in 300 μL of Milli-Q water (>18 Ω cm^{-1}) containing 10 mM spin-trapping agent 5-*tert*-butoxycarbonyl-5-methyl-1-pyrroline-*N*-oxide (BMPO). The extracts were then concentrated by a factor of 10–20 by evaporating water under N_2 gas for 10–13 min. The concentrated extracts were then loaded in a 50 μL capillary tube for EPR measurements at 24 minutes after extraction. Please note that the extracts were not filtered and they may contain both soluble and insoluble components. The EPR parameters used for ROS measurement were the same as those for EPFRs except a microwave frequency of 9.87 GHz; a magnetic field scan of 150 G; a modulation amplitude of 1 G; a time constant of 20.48 ms. The SpinFit and SpinCount modules in Xenon software were applied to simulate each EPR spectrum to identify and quantify different radical adducts.

Total dithiothreitol activities (OP-DTT)

The other half of each filter sample was extracted in 1.4–2.8 mL of Milli-Q water and analyzed with the DTT assay following our previous work.[52] The extracts and the filter were incubated with DTT (0.1 mM initial DTT concentration in the mixture) at 37 °C and pH 7.4. At different time intervals, an aliquot of the mixture was withdrawn and mixed with DTNB (5,5-dithio-bis-(2-nitrobenzoic acid)) and Tris buffer to determine the consumption rates of DTT over time. The total OP-DTT was calculated from the consumption rates of DTT normalized to total air sampled or mass of PM.

Laboratory pyrolysis and flaming combustion experiments. Canary island pine (*Pinus canariensis*), commonly planted in California (tree database, Arbor day Foundation), was used in pyrolysis and flaming combustion experiments (Fig. 1B and C). Pyrolysis PM samples were generated using a pyrolysis chamber consisting of a 2.5 cm quartz tube inside a Thermolyne 21135 tube furnace. Pine needles (about 0.3 g) were placed in a ceramic pyrolysis boat inside the quartz tube, flushed with nitrogen gas for 10 min (flow rate 0.9–1 L min^{-1}), and then inserted in the furnace. The temperature of the furnace was raised up to 300 °C with a starting pressure of ~750 Torr. Once the temperature reached 300 °C, the furnace was turned off. Smoke from pyrolysis was sent though a 47 mm filter folder containing a Teflon filter (Millipore Fluoropore Membrane Filter, PTFE, 0.2 μm pore size, FGLP04700) at a flow rate of ~1 L min^{-1}. After the pressure reached 850–900 torr, the collection was stopped to prevent overloading the filter, resulting in the heating time for pyrolysis to be about 10–15 minutes. For flaming combustion, pine needles were burned under atmospheric pressure in a portable kettle charcoal grill (Weber, P/N 40020) inside a standard 55-gallon steel drum. The grill damper on the lid of the charcoal grill was kept open all the time. Approximately 10 g of pine needles were placed on the cooking grate of the charcoal grill and lit on fire. The steel drum was then closed and a Teflon tube that connects to a sampling device (HI-Q environmental products continuous duty air sampling system; model no. LF2032-50) was suspended into the steel drum through a hole on its lid to collect the particles from the burning onto Teflon filters at a flow rate of 8 L min^{-1} for 15 min. The flaming continued for about 1 min, generating sufficient PM mass for analysis. Six PM samples from pyrolysis and flaming combustion were collected for analysis. EPFR, ROS, and OP-DTT measurements on these samples were conducted within one week of collection.

Results and discussion

Environmental persistent free radicals

Fig. 2A shows the representative EPR spectra of size-segregated PM samples collected during wildfire events and at the highway and urban sites without wildfires. The spectra for blank filters are similar to baselines without peaks. A paramagnetic species is characterized based on its *g* factor values and all spectra exhibit peaks near a *g* factor of 2, indicating the presence of EPFRs.[56,57] The mean and standard deviation of the *g* factor and peak-to-peak distance of the wildfire samples from all size ranges are 2.0028 ± 0.0003 and 6.2 ± 1.3 G, which are similar to those of highway (2.0026 ± 0.0006 and 7.7 ± 1.2 G) and urban (2.0031 ± 0.0005 and 5.8 ± 1.3 G) samples (Student's *t*-test, $p > 0.3$). The *g* factors are consistent with the values obtained previously from $PM_{2.5}$ samples collected simultaneously from the same highway and urban locations.[52] Generally, a *g* factor <2.003 corresponds to carbon-centered radicals and a higher value in the range of 2.003–2.004 represents carbon-centered

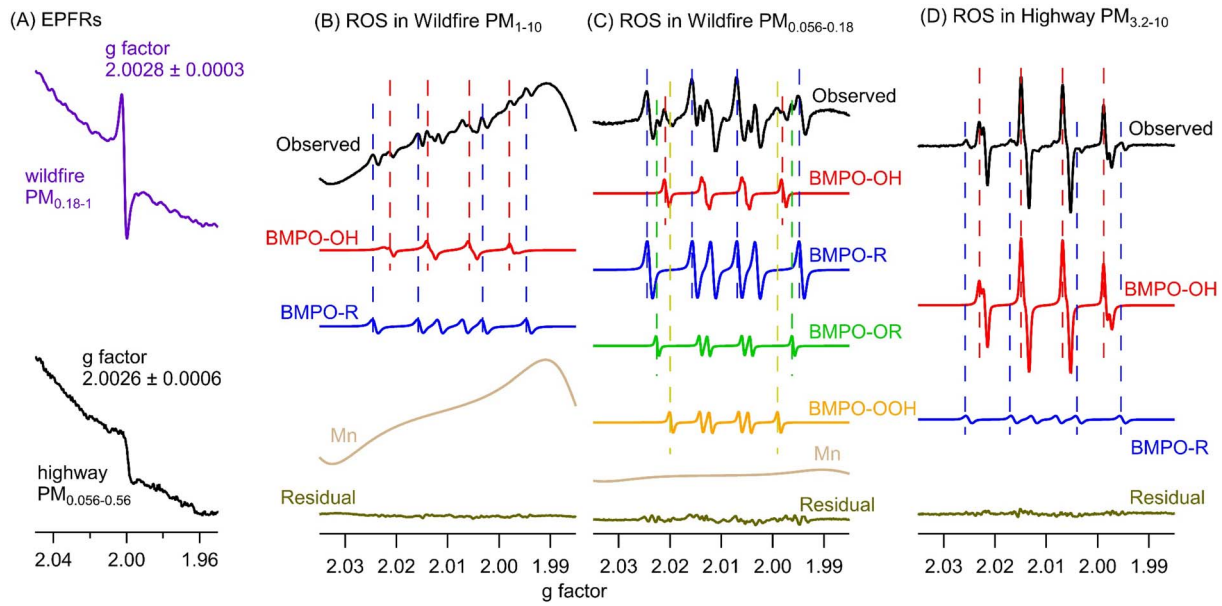

Fig. 2 (A) An example of EPR spectra showing the presence of EPFRs in ambient PM collected during a wildfire ($PM_{0.18-1}$ collected on Oct 26, 2020) and at the Long Beach highway site ($PM_{0.056-0.56}$ collected on Feb 8, 2020) as well as the average (± standard deviation) *g*-factors from wildfire and highway samples. (B–D) Examples of the observed EPR spectra (black) of the aqueous extracts of wildfire (B) PM_{1-10} and (C) $PM_{0.056-0.18}$ collected on Oct 26, 2020, and (D) highway $PM_{3.2-10}$ collected on Jan 31, 2020. The observed EPR spectra for ROS were simulated and deconvoluted to the spectrum of hydroxyl (·OH, red), carbon-centered (R·, blue), oxygen-centered (RO·, green), and superoxide or hydroperoxyl ($\cdot O_2^-/\cdot HO_2$, orange) radicals trapped by the spin-trapping agent BMPO, and manganese (Mn, Tan). The differences between the observed and simulated spectra are shown as residuals. The vertical dashed lines indicate the positions of characteristic peaks for BMPO radical adducts. EPFRs were directly measured on the PM filters and ROS formation was measured from the aqueous extracts.

radicals with adjacent oxygen atoms.[57] The observed *g* factors in this work indicate the presence of both types of radicals.

Fig. 3 shows the comparisons of EPFRs in wildfire, highway, and urban PM samples on frequency size distribution and average air-volume-normalized (EPFRv) and PM-mass-normalized concentrations (EPFRm) in PM_1 and PM_{1-10}. In all samples, EPFRs are predominantly found in submicron particles, while the urban and wildfire PM samples also show a small peak in the 10–18 μm size range (Fig. 3A). The average ambient concentrations of EPFRv in PM_1 (2.9–7.6 pmol m^{-3}) are much higher than those in PM_{1-10} (below the detection limit – 1.3 pmol m^{-3}) (Fig. 3B). Previous studies have shown that EPFRs can be found in both submicron and coarse modes.[54,68,69] Arangio *et al.* (2016)[68] and Wang *et al.* (2022)[69] found EPFRs mostly present in PM_1 in Mainz, a semi-urban site in Germany, and Xiamen, a coastal city in China, respectively. In contrast, Chen *et al.* (2020) found that EPFRs were mostly contained in coarse particles in winter and equally distributed in fine and coarse fractions in summer in Linfen, a typical coal-burning city in China.[54] EPFRv values in PM_1 from the wildfire samples are more than twice the EPFRv values in highway and urban samples, while EPFRm values are similar (~0.6 pmol μg^{-1}) and are also within the range of EPFRm in ambient PM of different sizes in previous studies.[61,68]

The similarity of the *g* factor, frequency size distribution, and EPFRm for wildfires and highway/urban sites suggests that the EPFRs in wildfire PM have similar radical species and properties to EPFRs in highway/urban PM. Our previous study[52] has shown good positive correlations of EPFRs with elemental carbon, carbon monoxide (CO, a combustion marker), and nitric oxide (NO, a traffic emission marker) in $PM_{2.5}$ collected at highway sites, suggesting that highway EPFRs were associated with diesel exhaust particles from incomplete combustion. In this work, the high abundance of EPFRs in submicron particles is consistent with the typical ambient mass size distribution of elemental carbon, a predominant fraction of soot,[70] peaking in the submicron size range.[71,72] Considering that particle-phase PAHs are abundant in submicron particles emitted from traffic-related combustion[73] and biomass burning as generated from thermal decomposition of organics upon incomplete combustion,[25,73–75] we speculate that some of the EPFRs from wildfire may be semiquinone radicals adsorbed on soot particles, which may be directly emitted from wildfires or secondary formed by oxidation of PAHs. EPFRs may also be stabilized by transition metals such as Fe and Cu ions,[57,58] which may also be contained in biomass burning PM.[20,76]

Reactive oxygen species formation

Fig. 2 also shows the typically observed and simulated EPR spectra of aqueous extracts of PM samples. The deconvolution of the EPR spectra allows us to identify the type of radical form of ROS based on hyperfine splitting constants and to estimate their relative contribution within each size range.[77] The hyperfine splitting constants of BMPO radical adducts elucidated from the simulations of the observed spectra are presented in Table S2.† For simplicity, the two BMPO-OH

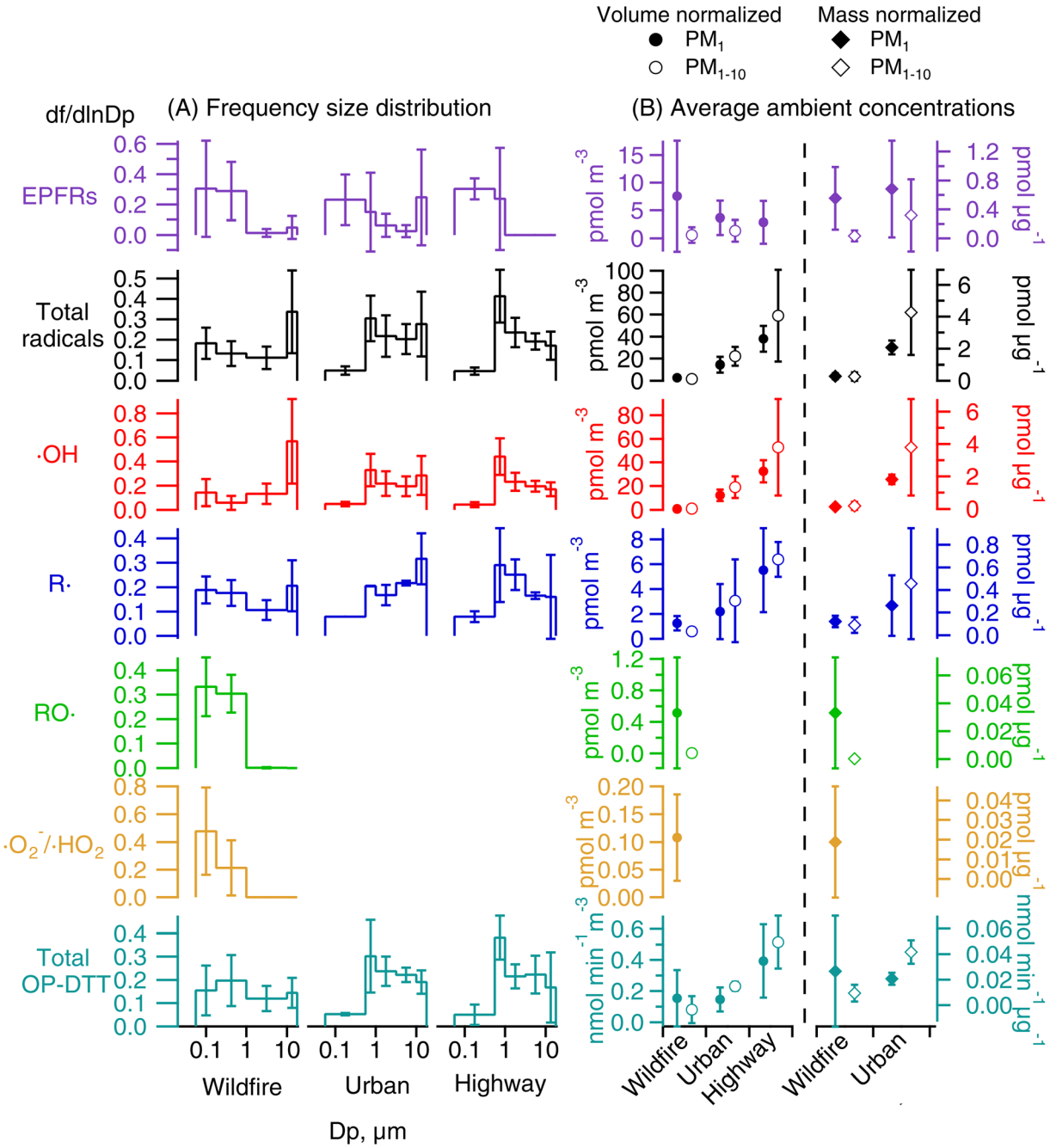

Fig. 3 (A) Average frequency distributions and (B) air volume-normalized (left axes) and PM mass-normalized concentrations (right axes) of EPFRs, ROS, and total OP-DTT of ambient PM collected during wildfire events and at highway and urban sites. Data are presented as mean and the standard deviation from different sampling days. PM_1 and PM_{1-10} are the sum of all MOUDI stages up to 1 μm and between 1 and 10 μm, respectively. PM mass concentrations are not available at the highway sites. RO· and $\cdot O_2^-/\cdot HO_2$ in highway and urban samples are below detection limits.

conformers were combined in Fig. 2B–D. Note that the distorted baselines in the EPR-ROS spectra of wildfire samples can be explained by the presence of paramagnetic manganese (Mn) species as evident from the 6-line signal in the metal region of the spectrum (Fig. S3†), which can be reproduced with a *g* value of 2.0086 (±0.0003) and hyperfine splitting constant of 96.5 (±1.7 G), characteristic for Mn.[78] It has been shown that biomass burning aerosols contain substantial amounts of Mn from mobilization of soil and dust particles during intensive fires.[1,20] Mn was not observed in any highway and urban samples. Our EPR measurements show that ambient PM at all particle sizes in wildfire, highway, and urban samples form hydroxyl (·OH) and carbon-centered (R·) radicals in the aqueous phase, while wildfire PM_1 can also form superoxide or hydroperoxyl radicals ($\cdot O_2^-/\cdot HO_2$) and oxygen-centered organic radicals (RO·).

As shown in Fig. 3A, ROS generated by wildfire PM have distinct frequency size distributions compared to those in highway and urban PM. The total radical forms of ROS (·OH, $\cdot O_2^-/\cdot HO_2$, RO·, and R·) in wildfire particles show a bimodal distribution with one peak at small sizes (0.056–0.18 μm) and the other peak at large sizes (10–18 μm), whereas the total radical forms of ROS in highway PM exhibit a single mode peaking in the 0.56–1 μm size range and urban PM has another peak at 10–18 μm. The ambient concentrations of ROSv in PM_1 and PM_{1-10} follow the order of highway > urban > wildfire (Fig. 3B). In terms of ROSm, the urban PM has much higher levels in PM_1 and PM_{1-10} compared to the wildfire PM. These results suggest that wildfire emissions lead to less total radical formation compared to traffic emissions. This may be because biomass burning PM contains a number of pyrolyzed, less oxidized, and insoluble components as well as inorganics such as potassium and sulfate which are not redox active.[79,80]

ROS from highway and urban background are predominantly composed of ·OH (84–88%, Fig. 4) with 12–16% contribution from R· for both PM_1 and PM_{1-10}. The dominant contribution of ·OH in ROS formation at highway and urban particles is also supported by ·OH and total radical forms of ROS showing very similar size distributions, ROSm levels, and a tight correlation (correlation coefficient $r^2 = 0.99$, Fig. S4A†). In contrast, for the wildfire PM, ·OH and R· have roughly equal contribution (~50%) to the total radical forms of ROS in PM_{1-10}, whereas in PM_1, R· (54%) and ·OH (28%) contribute substantially with some contribution from RO· (13%) and $\cdot O_2^-/\cdot HO_2$ (5%). The correlation between ·OH and total radical forms of ROS from the wildfire PM is strong for particle sizes larger than 1 μm ($r^2 = 0.89$), while the correlation for PM_1 is weaker ($r^2 = 0.40$, Fig. S4B†). R· has a similar frequency size distribution as total radicals and ·OH for all sites. RO· and $\cdot O_2^-/\cdot HO_2$ are mainly associated with PM_1 with a unimodal distribution that peaks at 0.056–0.18 μm. Their ROSv and ROSm in PM_1 are much higher than those of PM_{1-10}.

RO· and $\cdot O_2^-/\cdot HO_2$ are only observed in wildfire PM_1. In Fig. 5A and B, RO· shows a strong correlation with the total radical forms of ROS ($r^2 = 0.71$) and a moderate correlation with R· ($r^2 = 0.53$). $\cdot O_2^-/\cdot HO_2$ is moderately correlated with the total radical forms of ROS ($r^2 = 0.41$) and ·OH ($r^2 = 0.50$), but is not correlated with RO· or R·. The correlations among different radical species suggest that the organic radicals (RO· and R·) would be associated with similar aqueous chemistry that may be distinct from the formation chemistry of ·OH and $\cdot O_2^-/\cdot HO_2$. Biomass burning has been found to be an important primary source for organic hydroperoxides (ROOH).[81,82] The decomposition of ROOH can generate alkoxyl and OH radicals.[26,30,31,83] Alkoxyl radicals can undergo decomposition (*e.g.*, RO· → R′· + R″C(O)H) and isomerization (*e.g.*, RO· → (OH)R·) to form alkyl radicals,[84] whereas ·OH oxidizes primary or secondary alcohols to form α-hydroxyalkyl radicals followed by O_2 addition to form α-hydroxyperoxyl radicals that may decompose to form $\cdot O_2^-/\cdot HO_2$.[85] The correlations between ·OH and $\cdot O_2^-/\cdot HO_2$ may also be explained by a common role of iron ions in the decomposition H_2O_2 to form ·OH and reduction of O_2 to form $\cdot O_2^-$;[86,87] synergistically, these Fe-mediated ·OH and $\cdot O_2^-$ formation may be enhanced by the presence of HULIS and quinones in biomass burning PM.[33,88,89] Other chemical components in biomass burning may also explain the ROS formation: for example, organic peroxides (ROOR) can react with iron ions to form organic radicals;[29] Fe-organic complexes may release ROS by photolytic reactions;[90] and EPFRs can also reduce the molecular oxygen to form $\cdot O_2^-$.[62] Overall, the observed ROS formation should be a consequence of highly complex chemistry involving a variety of reactive and redox-active components in biomass burning PM; future laboratory studies are warranted to characterize specific ROS formation pathways and to investigate the interplay of different components with surrogate mixtures with known PM components.

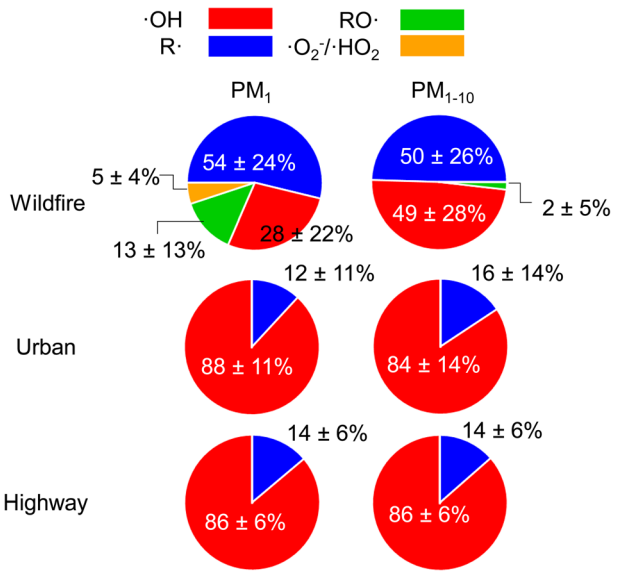

Fig. 4 Averaged fractions of ·OH, R·, RO·, and $\cdot O_2^-/\cdot HO_2$ in total radical formation in the aqueous extracts of PM_1 and PM_{1-10} collected during wildfire events and at highway and urban sites. RO· and $\cdot O_2^-/\cdot HO_2$ in highway and urban samples are below detection limits.

Total OP-DTT

As shown in Fig. 3, for total OP-DTT for highway and urban PM, a unimodal distribution with the peak at 0.56–1 μm is observed and total OP-DTT in PM_{1-10} is higher than that in PM_1. The highway PM has higher levels of total OP-DTTv than the urban PM, which may be partly caused by non-exhaust emissions of transition metals with large oxidative potential at highways.[38,91–93] The distribution of total OP-DTT for wildfire PM is relatively uniform across different particle diameter ranges and submicron wildfire PM exhibits higher total OP-DTTv and OP-DTTm compared to coarse fractions (Fig. 3). It is worth noting that wildfire PM shows higher contribution from submicron particles to EPFRs, ROS formation, and total OP-DTT compared to highway and urban PM. This observation is consistent with the fact that DTT-active organics including quinones and HULIS[45,46] are mostly contained in the submicron size range.[94,95] Since submicron particles after inhalation can deposit deep into the lung reaching the alveoli,[65] it suggests that biomass burning PM

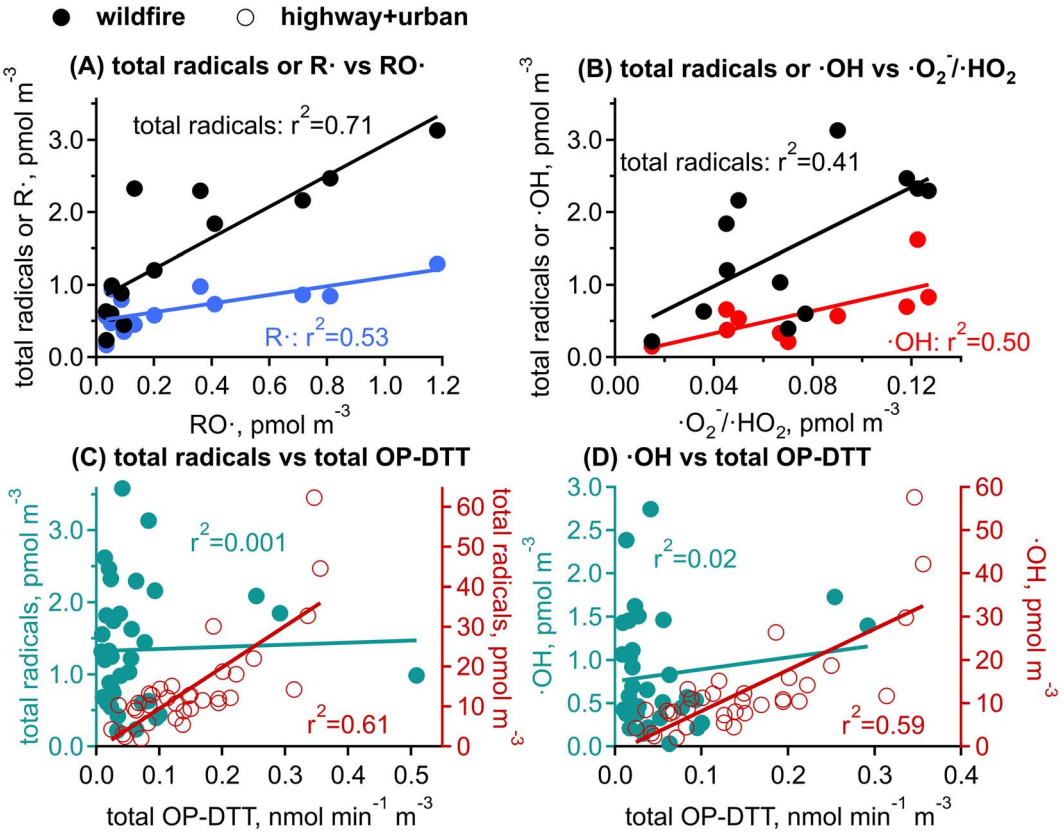

Fig. 5 Correlations of (A) total radicals and R· with RO· and (B) total radicals and ·OH with $\cdot O_2^-/\cdot HO_2$ during wildfire events; correlations of (C) total radicals with total OP-DTT and (D) ·OH with total OP-DTT during wildfire events and at highway/urban sites. Each data point represents data obtained from individual MOUDI stage.

can contribute to ROS formation in the lower respiratory tract and hence may play a role in inducing inflammatory responses and oxidative stress deeper in the lungs.

So far, the ambient size distributions of OP-DTT reported in the literature have been mostly focused on the water-soluble fraction.[96,97] Limited studies are available for total OP-DTT, which includes contributions from both water-soluble and -insoluble fractions. Insoluble PM components can also contribute to OP-DTT with health implications. Therefore, measuring total activities is important especially for wildfire PM as wildfire emission likely contains many insoluble components. Several studies used the Versatile Aerosol Concentration Enrichment System (VACES) to collect highly concentrated liquid suspensions of PM into different size fractions including quasi-ultrafine (<0.18 μm), accumulation (0.18–2.5 μm), and coarse (>2.5 μm) fractions, observing that the quasi-ultrafine fraction generally exhibited the greatest OP on a per particle mass basis.[98–100] In contrast, Charrier *et al.* (2015) obtained the total fraction of PM by combining the extracts of filter samples in water and organic solvents, and found that submicron particles (0.17–1 μm diameter) had the highest OP-DTTm.[101] Another study in Atlanta used the same protocol as in this work to measure total OP-DTT, showing a single mode distribution that peaks at ~1 μm from the urban background and a single coarse mode distribution at a road-side site.[102]

OP-DTT has been extensively used to indicate toxicity, assuming that it represents the ability of PM to generate ROS; this assumption still needs to be evaluated by investigating correlations between OP-DTT and ROS formation.[35,52,89,103] Interestingly, total OP-DTT from highway and urban sites shows a positive moderate correlation with the total radical forms of ROS ($r^2 = 0.61$, Fig. 5C) and ·OH ($r^2 = 0.59$, Fig. 5D), while total OP-DTT from wildfire samples does not correlate with any radical generation ($r^2 \leq 0.02$). The correlation in highway/urban PM samples may be explained by transition metals such as Cu or Fe that can oxidize DTT[47,48] and also participate in Fenton/Fenton-like reactions with H_2O_2 or hydroperoxides to generate ·OH.[30,104] Previous studies have also found mixed results for such correlation analysis. For example, Zhang *et al.* (2022) found that OP-DTT and ROS measurements were positively correlated for photochemically aged naphthalene SOA with soot particles, while there was a weaker correlation for β-pinene SOA.[103] Xiong *et al.* (2017) found that ambient $PM_{2.5}$ samples collected from an urban site in Illinois showed no correlation between OP-DTT and ·OH formation.[89] We previously observed positive correlations between OP-DTT and radical forms of ROS, ·OH, and organic radicals from aqueous extracts of $PM_{2.5}$ collected at the Anaheim highway site but not at the Long Beach site.[52] Ambient size distribution measurements on PM components combined with kinetic modeling incorporating ROS

chemistry in epithelial lung fluid suggested that OP-DTT is a good indicator of the chemical production of H_2O_2 and $\cdot O_2^-$, but does not represent $\cdot$OH generation.[35] The lack of correlation between OP-DTT and total radical forms of ROS in wildfire PM in this work indicates that OP measured with the DTT assay may not be a good metric for radical generation in biomass burning PM. This study only employed one OP assay and did not measure the non-radical forms of ROS such as H_2O_2, singlet oxygen ($^1O_2$) and triplet state organics, which can be formed by biomass burning photochemistry;[105–108] further studies should be conducted by applying different OP assays (*e.g.*, assays using ascorbic acid or glutathione) and comprehensive ROS measurements are necessary to fully evaluate the validations and limitations of the use of OP as an indicator of ROS formation and PM toxicity.

Effects of combustion conditions

In order to gain insights into the influence of burning conditions on EPFRs, ROS formation, and total OP-DTT, we conducted laboratory experiments to generate biomass burning PM under two combustion conditions: pyrolysis and flaming using pine needles. As shown in Fig. 6, flaming combustion produces much higher levels of mass-normalized EPFRs, ROS, and total OP-DTT in PM compared to pyrolysis. As pyrolysis occurs in the absence of oxygen and flaming involves consumption of oxygen, it suggests that the incorporation of oxygen upon production of biomass species may contribute to the reactivity and redox activity of biomass burning PM. The pyrolysis temperature (300 °C) used in this work is expected to produce mostly distillation products in the particles, *i.e.*, organic compounds present in the fuel, which may not be especially active in EPFRs or ROS activity.[109] In contrast, the emitted components are heavily oxidized under the flaming conditions. Note that the flaming phase in our experiment was roughly one minute after ignition and smoldering also likely occurred. One sample collected during the first minute of burning shows higher intrinsic activities than the average from all flaming samples (Fig. 6), which further supports that flaming produces aerosols with higher radical generation and OP than those from smoldering. The *g* factors of EPFRs for pyrolysis (2.0033 ± 0.0004) and flaming (2.0031 ± 0.0001) are similar and are close to the *g* factor from the wildfire PM, suggesting that the chemical identity of EPFRs should be very similar. Flaming combustion of pine needles only produces $\cdot$OH, while organic and $\cdot O_2^-$/$\cdot HO_2$ are also observed in ambient wildfire PM. In contrast, a previous study in Singapore reported that $PM_{2.5}$ collected during bush fires only generated $\cdot$OH.[7] Compared to the ambient wildfire PM, flaming-generated PM shows higher intrinsic levels of EPFRs and total OP-DTT but significantly lower $\cdot$OH generation, suggesting that flaming-dominated combustion can be a primary source for EPFRs and OP. Note that the biofuels in wildfires are more complex than the single species used in this experiment, which may be the reason for the distinctive differences in EFPRs, total OP-DTT, and the type of ROS formed between wildfire and flaming samples. In fact, a recent study found that fuel type was a primary factor controlling EPFR discharge from solid fuel combustion.[60] Another study that used a different fuel type (agricultural residues) found that OP-DTT and ROS of particles collected from open burning of rice straw and husk correlated well with water-insoluble organic carbon, suggesting that OP and ROS of the particles are largely impacted by water-insoluble OC components emitted under non-flaming combustion.[110] Thus, future studies are required to further characterize EPFRs, ROS formation, and OP of biomass burning PM as generated by various fuels and different combustion conditions, connecting these properties with the toxicity and health effects of wildfire PM.

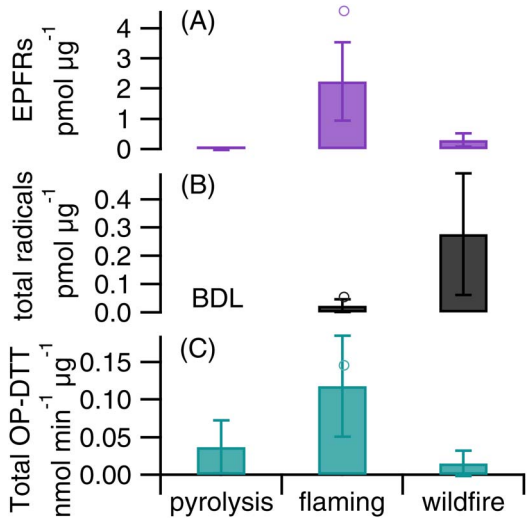

Fig. 6 PM mass-normalized concentrations (mean ± SD) of (A) EPFRs, (B) total radicals and (C) total OP-DTT of laboratory-generated particles from pyrolysis and flaming of pine needles, as well as ambient wildfire particles. The values for wildfire particles are sums of all MOUDI stages up to 10 μm and normalized by PM mass concentrations in PM_{10}. BDL – below detection limit. ○ – flaming sample collected during the first minute of burning.

Conclusions

Wildfires emit massive amounts of PM in the atmosphere and it is important to characterize their properties for evaluating their impacts on air quality and public health. In this study, we measured EPFRs, ROS formation upon dissolution in water and oxidative potential associated with ambient PM collected during two wildfire events. We observed that the submicron particles generated by wildfires contain substantial amounts of stable organic radicals, EPFRs. Upon interaction with water, wildfire PM can generate short-lived ROS including $\cdot$OH, superoxide, carbon-centered and oxygen-centered organic radicals. We found that combustion conditions can strongly impact EPFRs and ROS formation, with flaming conditions generating much more of these species compared to smoldering/pyrolysis conditions. While it has been suggested that PM oxidative potential would be a good indicator of PM toxicity, we found that radical formation by wildfire PM exhibit little correlations with oxidative potential measured by the DTT

assay. Further studies are warranted to measure the non-radical forms of ROS (*e.g.*, H_2O_2) and other toxicological endpoints to evaluate the connection between EPFRs, ROS, OP, and PM toxicity and better assessments of PM impacts on air quality and public health.

Author contributions

TF, SN and MS conceptualized the experiment; TF, BH, SK, KH, JW and VN were involved in the data collection; TF, BCHH and SK analyzed the data; TF wrote the manuscript, and all authors edited the manuscript.

Conflicts of interest

All authors declare no competing interests.

Acknowledgements

The research described in this article was conducted under contract to the Health Effects Institute (HEI) (Walter A. Rosenblith New Investigator Award, no. 4964-RFA17-3/18-6), an organization jointly funded by the United States Environmental Protection Agency (EPA) (Assistance Award no. CR-83590201) and certain motor vehicle and engine manufacturers. The contents of this article neither necessarily reflect the views of HEI, or its sponsors, nor do they necessarily reflect the views and policies of the EPA or motor vehicle and engine manufacturers. We acknowledge funding from the National Science Foundation (CHE-2203419) and from the Japan Automobile Research Institute (5606855). We also acknowledge Prof. Heejung Jung from the University of California, Riverside and Prof. Xiaoliang Wang from the Desert Research Institute for their help in PM sampling at the highway sites. We also acknowledge the South Coast Air Quality Management District (SCAQMD) for providing their highway site for PM sampling.

References

1 R. Wagner, M. Jähn and K. Schepanski, Wildfires as a source of airborne mineral dust – revisiting a conceptual model using large-eddy simulation (LES), *Atmos. Chem. Phys.*, 2018, **18**(16), 11863–11884.
2 W. J. Bond, F. I. Woodward and G. F. Midgley, The global distribution of ecosystems in a world without fire, *New Phytol.*, 2005, **165**(2), 525–538.
3 A. L. Westerling, H. G. Hidalgo, D. R. Cayan and T. W. Swetnam, Warming and Earlier Spring Increase Western U.S. Forest Wildfire Activity, *Science*, 2006, **313**(5789), 940–943.
4 D. A. Jaffe, S. M. O'Neill, N. K. Larkin, A. L. Holder, D. L. Peterson, J. E. Halofsky and A. G. Rappold, Wildfire and prescribed burning impacts on air quality in the United States, *J. Air Waste Manage. Assoc.*, 2020, **70**(6), 583–615.
5 R. Xu, P. Yu, M. J. Abramson, F. H. Johnston, J. M. Samet, M. L. Bell, A. Haines, K. L. Ebi, S. Li and Y. Guo, Wildfires, Global Climate Change, and Human Health, *N. Engl. J. Med.*, 2020, **383**(22), 2173–2181.
6 V. Verma, A. Polidori, J. J. Schauer, M. M. Shafer, F. R. Cassee and C. Sioutas, Physicochemical and toxicological profiles of particulate matter in Los Angeles during the October 2007 southern California wildfires, *Environ. Sci. Technol.*, 2009, **43**(3), 954–960.
7 S. Karthikeyan, R. Balasubramanian and K. Iouri, Particulate Air Pollution from Bushfires: Human Exposure and Possible Health Effects, *J. Toxicol. Environ. Health, Part A*, 2006, **69**(21), 1895–1908.
8 M. Pardo, C. Li, Q. He, S. Levin-Zaidman, M. Tsoory, Q. Yu, X. Wang and Y. Rudich, Mechanisms of lung toxicity induced by biomass burning aerosols, *Part. Fibre Toxicol.*, 2020, **17**(1), 4.
9 Y. Liang, D. Sengupta, M. J. Campmier, D. M. Lunderberg, J. S. Apte and A. H. Goldstein, Wildfire smoke impacts on indoor air quality assessed using crowdsourced data in California, *Proc. Natl. Acad. Sci. U. S. A.*, 2021, **118**(36), e2106478118.
10 J. A. Sarnat, A. Marmur, M. Klein, E. Kim, A. G. Russell, S. E. Sarnat, J. A. Mulholland, P. K. Hopke and P. E. Tolbert, Fine particle sources and cardiorespiratory morbidity: an application of chemical mass balance and factor analytical source-apportionment methods, *Environ. Health Perspect.*, 2008, **116**(4), 459–466.
11 A. J. Ghio, Mechanism of asthmatic exacerbation by ambient air pollution particles, *Expert Rev. Respir. Med.*, 2008, **2**(1), 109–118.
12 R. J. Delfino, S. Brummel, J. Wu, H. Stern, B. Ostro, M. Lipsett, A. Winer, D. H. Street, L. Zhang, T. Tjoa and D. L. Gillen, The relationship of respiratory and cardiovascular hospital admissions to the southern California wildfires of 2003, *Occup. Environ. Med.*, 2009, **66**(3), 189–197.
13 X. Zhou, K. Josey, L. Kamareddine, C. Caine Miah, T. Liu, J. Mickley Loretta, M. Cooper and F. Dominici, Excess of COVID-19 cases and deaths due to fine particulate matter exposure during the 2020 wildfires in the United States, *Sci. Adv.*, 2021, **7**(33), eabi8789.
14 O. Pechony and D. T. Shindell, Driving forces of global wildfires over the past millennium and the forthcoming century, *Proc. Natl. Acad. Sci. U. S. A.*, 2010, **107**(45), 19167–19170.
15 K. J. A. Davies, Oxidative stress: the paradox of aerobic life, *Biochem. Soc. Symp.*, 1995, **61**, 1.
16 S. V. Lakshmi, G. Padmaja, P. Kuppusamy and V. K. Kutala, Oxidative stress in cardiovascular disease, *Indian J. Biochem. Biophys.*, 2009, **46**(6), 421–440.
17 M. Schieber and N. S. Chandel, ROS function in redox signaling and oxidative stress, *Curr. Biol.*, 2014, **24**(10), R453–R462.
18 M. Shiraiwa, K. Ueda, A. Pozzer, G. Lammel, C. J. Kampf, A. Fushimi, S. Enami, A. M. Arangio, J. Fröhlich-Nowoisky, Y. Fujitani, A. Furuyama, P. S. J. Lakey, J. Lelieveld, K. Lucas, Y. Morino, U. Pöschl, S. Takahama, A. Takami, H. Tong, B. Weber, A. Yoshino and K. Sato,

Aerosol Health Effects from Molecular to Global Scales, *Environ. Sci. Technol.*, 2017, **51**(23), 13545–13567.

19 S. Arciva, C. Niedek, C. Mavis, M. Yoon, M. E. Sanchez, Q. Zhang and C. Anastasio, Aqueous ·OH Oxidation of Highly Substituted Phenols as a Source of Secondary Organic Aerosol, *Environ. Sci. Technol.*, 2022, **56**(14), 9959–9967.

20 G. Jahn Leif, J. Polen Michael, G. Jahl Lydia, A. Brubaker Thomas, J. Somers and C. Sullivan Ryan, Biomass combustion produces ice-active minerals in biomass-burning aerosol and bottom ash, *Proc. Natl. Acad. Sci.*, 2020, **117**(36), 21928–21937.

21 B. B. Palm, Q. Peng, D. Fredrickson Carley, H. Lee Ben, A. Garofalo Lauren, A. Pothier Matson, M. Kreidenweis Sonia, K. Farmer Delphine, P. Pokhrel Rudra, Y. Shen, M. Murphy Shane, W. Permar, L. Hu, L. Campos Teresa, R. Hall Samuel, K. Ullmann, X. Zhang, F. Flocke, V. Fischer Emily and A. Thornton Joel, Quantification of organic aerosol and brown carbon evolution in fresh wildfire plumes, *Proc. Natl. Acad. Sci.*, 2020, **117**(47), 29469–29477.

22 R. K. Chakrabarty, N. D. Beres, H. Moosmüller, S. China, C. Mazzoleni, M. K. Dubey, L. Liu and M. I. Mishchenko, Soot superaggregates from flaming wildfires and their direct radiative forcing, *Sci. Rep.*, 2014, **4**(1), 5508.

23 B. Y. Kuang, P. Lin, X. H. H. Huang and J. Z. Yu, Sources of humic-like substances in the Pearl River Delta, China: positive matrix factorization analysis of PM2.5 major components and source markers, *Atmos. Chem. Phys.*, 2015, **15**(4), 1995–2008.

24 A. Laskin, J. Laskin and S. A. Nizkorodov, Chemistry of Atmospheric Brown Carbon, *Chem. Rev.*, 2015, **115**(10), 4335–4382.

25 V. Samburova, J. Connolly, M. Gyawali, R. L. N. Yatavelli, A. C. Watts, R. K. Chakrabarty, B. Zielinska, H. Moosmüller and A. Khlystov, Polycyclic aromatic hydrocarbons in biomass-burning emissions and their contribution to light absorption and aerosol toxicity, *Sci. Total Environ.*, 2016, **568**, 391–401.

26 H. Tong, P. S. J. Lakey, A. M. Arangio, J. Socorro, F. Shen, K. Lucas, W. H. Brune, U. Pöschl and M. Shiraiwa, Reactive Oxygen Species Formed by Secondary Organic Aerosols in Water and Surrogate Lung Fluid, *Environ. Sci. Technol.*, 2018, **52**(20), 11642–11651.

27 P. H. Chowdhury, Q. He, R. Carmieli, C. Li, Y. Rudich and M. Pardo, Connecting the Oxidative Potential of Secondary Organic Aerosols with Reactive Oxygen Species in Exposed Lung Cells, *Environ. Sci. Technol.*, 2019, **53**(23), 13949–13958.

28 R. D. McWhinney, S. Zhou and J. P. D. Abbatt, Naphthalene SOA: redox activity and naphthoquinone gas–particle partitioning, *Atmos. Chem. Phys.*, 2013, **13**(19), 9731–9744.

29 J. Wei, T. Fang, P. S. J. Lakey and M. Shiraiwa, Iron-Facilitated Organic Radical Formation from Secondary Organic Aerosols in Surrogate Lung Fluid, *Environ. Sci. Technol.*, 2021.

30 T. Fang, P. S. J. Lakey, J. C. Rivera-Rios, F. N. Keutsch and M. Shiraiwa, Aqueous-Phase Decomposition of Isoprene Hydroxy Hydroperoxide and Hydroxyl Radical Formation by Fenton-like Reactions with Iron Ions, *J. Phys. Chem. A*, 2020, **124**(25), 5230–5236.

31 H. Tong, A. M. Arangio, P. S. J. Lakey, T. Berkemeier, F. Liu, C. J. Kampf, W. H. Brune, U. Pöschl and M. Shiraiwa, Hydroxyl Radicals from Secondary Organic Aerosol Decomposition in Water, *Atmos. Chem. Phys.*, 2016, **16**(3), 1761–1771.

32 S. E. Paulson, P. J. Gallimore, X. M. Kuang, J. R. Chen, M. Kalberer and D. H. Gonzalez, A Light-Driven Burst of Hydroxyl Radicals Dominates Oxidation Chemistry in Newly Activated Cloud Droplets, *Sci. Adv.*, 2019, **5**(5), eaav7689.

33 D. H. Gonzalez, C. K. Cala, Q. Peng and S. E. Paulson, HULIS Enhancement of Hydroxyl Radical Formation from Fe(II): Kinetics of Fulvic Acid–Fe(II) Complexes in the Presence of Lung Antioxidants, *Environ. Sci. Technol.*, 2017, **51**(13), 7676–7685.

34 B. Ervens, Modeling the Processing of Aerosol and Trace Gases in Clouds and Fogs, *Chem. Rev.*, 2015, **115**(10), 4157–4198.

35 T. Fang, P. S. J. Lakey, R. J. Weber and M. Shiraiwa, Oxidative Potential of Particulate Matter and Generation of Reactive Oxygen Species in Epithelial Lining Fluid, *Environ. Sci. Technol.*, 2019, **53**(21), 12784–12792.

36 L. He and J. Zhang, Particulate matter (PM) oxidative potential: Measurement methods and links to PM physicochemical characteristics and health effects, *Crit. Rev. Environ. Sci. Technol.*, 2022, 1–21.

37 J. T. Bates, R. J. Weber, J. Abrams, V. Verma, T. Fang, M. Klein, M. J. Strickland, S. E. Sarnat, H. H. Chang, J. A. Mulholland, P. E. Tolbert and A. G. Russell, Reactive Oxygen Species Generation Linked to Sources of Atmospheric Particulate Matter and Cardiorespiratory Effects, *Environ. Sci. Technol.*, 2015, **49**(22), 13605–13612.

38 T. Fang, V. Verma, J. T. Bates, J. Abrams, M. Klein, M. J. Strickland, S. E. Sarnat, H. H. Chang, J. A. Mulholland, P. E. Tolbert, A. G. Russell and R. J. Weber, Oxidative potential of ambient water-soluble PM2.5 in the southeastern United States: contrasts in sources and health associations between ascorbic acid (AA) and dithiothreitol (DTT) assays, *Atmos. Chem. Phys.*, 2016, **16**(6), 3865–3879.

39 Y. Ma, Y. Cheng, X. Qiu, G. Cao, Y. Fang, J. Wang, T. Zhu, J. Yu and D. Hu, Sources and oxidative potential of water-soluble humic-like substances (HULISWS) in fine particulate matter (PM2.5) in Beijing, *Atmos. Chem. Phys.*, 2018, **18**(8), 5607–5617.

40 S. Weber, G. Uzu, O. Favez, L. J. S. Borlaza, A. Calas, D. Salameh, F. Chevrier, J. Allard, J. L. Besombes, A. Albinet, S. Pontet, B. Mesbah, G. Gille, S. Zhang, C. Pallares, E. Leoz-Garziandia and J. L. Jaffrezo, Source apportionment of atmospheric PM10 oxidative potential: synthesis of 15 year-round urban datasets in France, *Atmos. Chem. Phys.*, 2021, **21**(14), 11353–11378.

41 K. R. Daellenbach, G. Uzu, J. Jiang, L.-E. Cassagnes, Z. Leni, A. Vlachou, G. Stefenelli, F. Canonaco, S. Weber, A. Segers, J. J. P. Kuenen, M. Schaap, O. Favez, A. Albinet, S. Aksoyoglu, J. Dommen, U. Baltensperger, M. Geiser, I. El Haddad, J.-L. Jaffrezo and A. S. H. Prévôt, Sources of particulate-matter air pollution and its oxidative potential in Europe, *Nature*, 2020, **587**(7834), 414–419.

42 M. Antinolo, M. D. Willis, S. Zhou and J. P. D. Abbatt, Connecting the oxidation of soot to its redox cycling abilities, *Nat. Commun.*, 2015, **6**, 6812.

43 S. Wang, J. Ye, R. Soong, B. Wu, L. Yu, A. J. Simpson and A. W. H. Chan, Relationship between chemical composition and oxidative potential of secondary organic aerosol from polycyclic aromatic hydrocarbons, *Atmos. Chem. Phys.*, 2018, **18**(6), 3987–4003.

44 M. Y. Chung, R. A. Lazaro, D. Lim, J. Jackson, J. Lyon, D. Rendulic and A. S. Hasson, Aerosol-borne quinones and reactive oxygen species generation by particulate matter extracts, *Environ. Sci. Technol.*, 2006, **40**(16), 4880–4886.

45 V. Verma, Y. Wang, R. El-Afifi, T. Fang, J. Rowland, A. G. Russell and R. J. Weber, Fractionating ambient humic-like substances (HULIS) for their reactive oxygen species activity – Assessing the importance of quinones and atmospheric aging, *Atmos. Environ.*, 2015, **120**, 351–359.

46 J. Dou, P. Lin, B.-Y. Kuang and J. Z. Yu, Reactive Oxygen Species Production Mediated by Humic-like Substances in Atmospheric Aerosols: Enhancement Effects by Pyridine, Imidazole, and Their Derivatives, *Environ. Sci. Technol.*, 2015, **49**(11), 6457–6465.

47 J. G. Charrier and C. Anastasio, On dithiothreitol (DTT) as a measure of oxidative potential for ambient particles: evidence for the importance of soluble transition metals, *Atmos. Chem. Phys.*, 2012, **12**(19), 9321–9333.

48 J. G. Charrier, A. S. McFall, K. K. Vu, J. Baroi, C. Olea, A. Hasson and C. Anastasio, A bias in the "mass-normalized" DTT response – an effect of non-linear concentration-response curves for copper and manganese, *Atmos. Environ.*, 2016, **144**, 325–334.

49 M. Lin and J. Z. Yu, Assessment of Interactions between Transition Metals and Atmospheric Organics: Ascorbic Acid Depletion and Hydroxyl Radical Formation in Organic-Metal Mixtures, *Environ. Sci. Technol.*, 2020, **54**(3), 1431–1442.

50 J. Wei, H. Yu, Y. Wang and V. Verma, Complexation of Iron and Copper in Ambient Particulate Matter and Its Effect on the Oxidative Potential Measured in a Surrogate Lung Fluid, *Environ. Sci. Technol.*, 2019, **53**(3), 1661–1671.

51 H. Yu, J. Wei, Y. Cheng, K. Subedi and V. Verma, Synergistic and Antagonistic Interactions among the Particulate Matter Components in Generating Reactive Oxygen Species Based on the Dithiothreitol Assay, *Environ. Sci. Technol.*, 2018, **52**(4), 2261–2270.

52 B. Hwang, T. Fang, R. Pham, J. Wei, S. Gronstal, B. Lopez, C. Frederickson, T. Galeazzo, X. Wang, H. Jung and M. Shiraiwa, Environmentally Persistent Free Radicals, Reactive Oxygen Species Generation, and Oxidative Potential of Highway PM2.5, *ACS Earth Space Chem.*, 2021, **5**(8), 1865–1875.

53 G. Sigmund, C. Santín, M. Pignitter, N. Tepe, S. H. Doerr and T. Hofmann, Environmentally persistent free radicals are ubiquitous in wildfire charcoals and remain stable for years, *Commun. Earth Environ.*, 2021, **2**(1), 68.

54 Q. Chen, H. Sun, W. Song, F. Cao, C. Tian and Y. L. Zhang, Size-resolved exposure risk of persistent free radicals (PFRs) in atmospheric aerosols and their potential sources, *Atmos. Chem. Phys.*, 2020, **20**(22), 14407–14417.

55 Q. Chen, H. Sun, Z. Mu, Y. Wang, Y. Li, L. Zhang, M. Wang and Z. Zhang, Characteristics of environmentally persistent free radicals in PM2.5: Concentrations, species and sources in Xi'an, Northwestern China, *Environ. Pollut.*, 2019, **247**, 18–26.

56 W. Gehling and B. Dellinger, Environmentally Persistent Free Radicals and Their Lifetimes in PM2.5, *Environ. Sci. Technol.*, 2013, **47**(15), 8172–8178.

57 B. Dellinger, S. Lomnicki, L. Khachatryan, Z. Maskos, R. W. Hall, J. Adounkpe, C. McFerrin and H. Truong, Formation and stabilization of persistent free radicals, *Proc. Combust. Inst.*, 2007, **31**(1), 521–528.

58 S. Lomnicki, H. Truong, E. Vejerano and B. Dellinger, Copper Oxide-Based Model of Persistent Free Radical Formation on Combustion-Derived Particulate Matter, *Environ. Sci. Technol.*, 2008, **42**(13), 4982–4988.

59 C. K. Borrowman, S. Zhou, T. E. Burrow and J. P. D. Abbatt, Formation of environmentally persistent free radicals from the heterogeneous reaction of ozone and polycyclic aromatic compounds, *Phys. Chem. Chem. Phys.*, 2016, **18**(1), 205–212.

60 J. Zhao, G. Shen, L. Shi, H. Li, D. Lang, L. Zhang, B. Pan and S. Tao, Real-World Emission Characteristics of Environmentally Persistent Free Radicals in PM2.5 from Residential Solid Fuel Combustion, *Environ. Sci. Technol.*, 2022, **56**(7), 3997–4004.

61 G. L. Squadrito, R. Cueto, B. Dellinger and W. A. Pryor, Quinoid redox cycling as a mechanism for sustained free radical generation by inhaled airborne particulate matter, *Free Radicals Biol. Med.*, 2001, **31**(9), 1132–1138.

62 L. Khachatryan, E. Vejerano, S. Lomnicki and B. Dellinger, Environmentally Persistent Free Radicals (EPFRs). 1. Generation of Reactive Oxygen Species in Aqueous Solutions, *Environ. Sci. Technol.*, 2011, **45**(19), 8559–8566.

63 L. Khachatryan and B. Dellinger, Environmentally Persistent Free Radicals (EPFRs)-2. Are Free Hydroxyl Radicals Generated in Aqueous Solutions?, *Environ. Sci. Technol.*, 2011, **45**(21), 9232–9239.

64 S. Balakrishna, S. Lomnicki, K. M. McAvey, R. B. Cole, B. Dellinger and S. A. Cormier, Environmentally persistent free radicals amplify ultrafine particle mediated cellular oxidative stress and cytotoxicity, *Part. Fibre Toxicol.*, 2009, **6**(1), 11.

65 J. Heyder, Deposition of Inhaled Particles in the Human Respiratory Tract and Consequences for Regional

Targeting in Respiratory Drug Delivery, *Proc. Am. Thorac. Soc.*, 2004, **1**(4), 315–320.

66 A. L. Hodshire, A. Akherati, M. J. Alvarado, B. Brown-Steiner, S. H. Jathar, J. L. Jimenez, S. M. Kreidenweis, C. R. Lonsdale, T. B. Onasch, A. M. Ortega and J. R. Pierce, Aging Effects on Biomass Burning Aerosol Mass and Composition: A Critical Review of Field and Laboratory Studies, *Environ. Sci. Technol.*, 2019, **53**(17), 10007–10022.

67 A. L. Hodshire, E. Ramnarine, A. Akherati, M. L. Alvarado, D. K. Farmer, S. H. Jathar, S. M. Kreidenweis, C. R. Lonsdale, T. B. Onasch, S. R. Springston, J. Wang, Y. Wang, L. I. Kleinman, A. J. Sedlacek Iii and J. R. Pierce, Dilution impacts on smoke aging: evidence in Biomass Burning Observation Project (BBOP) data, *Atmos. Chem. Phys.*, 2021, **21**(9), 6839–6855.

68 A. M. Arangio, H. Tong, J. Socorro, U. Pöschl and M. Shiraiwa, Quantification of Environmentally Persistent Free Radicals and Reactive Oxygen Species in Atmospheric Aerosol Particles, *Atmos. Chem. Phys.*, 2016, **16**(20), 13105–13119.

69 Y. Wang, K. Yao, X. e. Fu, X. Zhai, L. Jin and H. Guo, Size-resolved exposure risk and subsequent role of environmentally persistent free radicals (EPFRs) from atmospheric particles, *Atmos. Environ.*, 2022, **276**, 119059.

70 A. Y. Watson and P. A. Valberg, Carbon Black and Soot: Two Different Substances, *Am. Ind. Hyg. Assoc. J.*, 2001, **62**(2), 218–228.

71 T. Fang, H. Guo, L. Zeng, V. Verma, A. Nenes and R. J. Weber, Highly acidic ambient particles, soluble metals, and oxidative potential: a link between sulfate and aerosol toxicity, *Environ. Sci. Technol.*, 2017, **51**, 2611–2620.

72 T. C. Bond, S. J. Doherty, D. W. Fahey, P. M. Forster, T. Berntsen, B. J. DeAngelo, M. G. Flanner, S. Ghan, B. Kärcher, D. Koch, S. Kinne, Y. Kondo, P. K. Quinn, M. C. Sarofim, M. G. Schultz, M. Schulz, C. Venkataraman, H. Zhang, S. Zhang, N. Bellouin, S. K. Guttikunda, P. K. Hopke, M. Z. Jacobson, J. W. Kaiser, Z. Klimont, U. Lohmann, J. P. Schwarz, D. Shindell, T. Storelvmo, S. G. Warren and C. S. Zender, Bounding the role of black carbon in the climate system: A scientific assessment, *J. Geophys. Res.: Atmos.*, 2013, **118**(11), 5380–5552.

73 T. Lu, Z. Huang, C. S. Cheung and J. Ma, Size distribution of EC, OC and particle-phase PAHs emissions from a diesel engine fueled with three fuels, *Sci. Total Environ.*, 2012, **438**, 33–41.

74 B. Zielinska, J. Sagebiel, W. P. Arnott, C. F. Rogers, K. E. Kelly, D. A. Wagner, J. S. Lighty, A. F. Sarofim and G. Palmer, Phase and Size Distribution of Polycyclic Aromatic Hydrocarbons in Diesel and Gasoline Vehicle Emissions, *Environ. Sci. Technol.*, 2004, **38**(9), 2557–2567.

75 C. Venkataraman, J. M. Lyons and S. K. Friedlander, Size Distributions of Polycyclic Aromatic Hydrocarbons and Elemental Carbon. 1. Sampling, Measurement Methods, and Source Characterization, *Environ. Sci. Technol.*, 1994, **28**(4), 555–562.

76 A. L. Chang-Graham, L. T. M. Profeta, T. J. Johnson, R. J. Yokelson, A. Laskin and J. Laskin, Case study of water-soluble metal containing organic constituents of biomass burning aerosol, *Environ. Sci. Technol.*, 2011, **45**(4), 1257–1263.

77 A. Misak, V. Brezova, M. Grman, L. Tomasova, M. Chovanec and K. Ondrias, (•)BMPO-OOH Spin-Adduct as a Model for Study of Decomposition of Organic Hydroperoxides and the Effects of Sulfide/Selenite Derivatives. An EPR Spin-Trapping Approach, *Antioxidants*, 2020, **9**(10), 918.

78 A. K. Kar, A. Acharya, G. C. Pradhan and A. C. Dash, Glyoxylate as a reducing agent for manganese(III) in salen scaffold: A kinetics and mechanistic study, *J. Chem. Sci.*, 2014, **126**(3), 547–559.

79 C. Khamkaew, S. Chantara, R. Janta, S. K. Pani, T. Prapamontol, S. Kawichai, W. Wiriya and N.-H. Lin, Investigation of Biomass Burning Chemical Components over Northern Southeast Asia during 7-SEAS/BASELInE 2014 Campaign, *Aerosol Air Qual. Res.*, 2016, **16**(11), 2655–2670.

80 W. Li, P. Ge, M. Chen, J. Tang, M. Cao, Y. Cui, K. Hu and D. Nie, Tracers from Biomass Burning Emissions and Identification of Biomass Burning, *Atmosphere*, 2021, **12**(11).

81 M. Lee, B. G. Heikes, D. J. Jacob, G. Sachse and B. Anderson, Hydrogen peroxide, organic hydroperoxide, and formaldehyde as primary pollutants from biomass burning, *J. Geophys. Res.: Atmos.*, 1997, **102**(D1), 1301–1309.

82 J. A. Snow, B. G. Heikes, H. Shen, D. W. O'Sullivan, A. Fried and J. Walega, Hydrogen peroxide, methyl hydroperoxide, and formaldehyde over North America and the North Atlantic, *J. Geophys. Res.: Atmos.*, 2007, **112**, D12S07.

83 K. M. Badali, S. Zhou, D. Aljawhary, M. Antiñolo, W. J. Chen, A. Lok, E. Mungall, J. P. S. Wong, R. Zhao and J. P. D. Abbatt, Formation of Hydroxyl Radicals from Photolysis of Secondary Organic Aerosol Material, *Atmos. Chem. Phys.*, 2015, **15**(14), 7831–7840.

84 Q. Chen, Y. Liu, N. M. Donahue, J. E. Shilling and S. T. Martin, Particle-Phase Chemistry of Secondary Organic Material: Modeled Compared to Measured O:C and H:C Elemental Ratios Provide Constraints, *Environ. Sci. Technol.*, 2011, **45**(11), 4763–4770.

85 J. Wei, T. Fang, C. Wong, P. S. J. Lakey, S. A. Nizkorodov and M. Shiraiwa, Superoxide Formation from Aqueous Reactions of Biogenic Secondary Organic Aerosols, *Environ. Sci. Technol.*, 2021, **55**(1), 260–270.

86 H. J. H. Fenton, LXXIII.—Oxidation of Tartaric Acid in Presence of Iron, *J. Chem. Soc., Trans.*, 1894, **65**, 899–910.

87 J. M. Santana-Casiano, M. González-Dávila and F. J. Millero, Oxidation of Nanomolar Levels of Fe(II) with Oxygen in Natural Waters, *Environ. Sci. Technol.*, 2005, **39**(7), 2073–2079.

88 J. G. Charrier and C. Anastasio, Rates of Hydroxyl Radical Production from Transition Metals and Quinones in

a Surrogate Lung Fluid, *Environ. Sci. Technol.*, 2015, **49**(15), 9317–9325.

89 Q. Xiong, H. Yu, R. Wang, J. Wei and V. Verma, Rethinking Dithiothreitol-Based Particulate Matter Oxidative Potential: Measuring Dithiothreitol Consumption *versus* Reactive Oxygen Species Generation, *Environ. Sci. Technol.*, 2017, **51**(11), 6507–6514.

90 P. A. Alpert, J. Dou, P. Corral Arroyo, F. Schneider, J. Xto, B. Luo, T. Peter, T. Huthwelker, C. N. Borca, K. D. Henzler, T. Schaefer, H. Herrmann, J. Raabe, B. Watts, U. K. Krieger and M. Ammann, Photolytic radical persistence due to anoxia in viscous aerosol particles, *Nat. Commun.*, 2021, **12**(1), 1769.

91 D. Gao, T. Fang, V. Verma, L. Zeng and R. Weber, A method for measuring total aerosol oxidative potential (OP) with the dithiothreitol (DTT) assay and comparisons between an urban and roadside site of water-soluble and total OP, *Atmos. Meas. Tech.*, 2017, **2017**, 1–25.

92 A. Saffari, N. Daher, M. M. Shafer, J. J. Schauer and C. Sioutas, Seasonal and spatial variation in dithiothreitol (DTT) activity of quasi-ultrafine particles in the Los Angeles Basin and its association with chemical species, *J. Environ. Sci. Health, Part A: Toxic/Hazard. Subst. Environ. Eng.*, 2014, **49**(4), 441–451.

93 X. Zhang, N. Staimer, T. Tjoa, D. L. Gillen, J. J. Schauer, M. M. Shafer, S. Hasheminassab, P. Pakbin, J. Longhurst, C. Sioutas and R. J. Delfino, Associations between microvascular function and short-term exposure to traffic-related air pollution and particulate matter oxidative potential, *Environ. Health*, 2016, **15**(1), 81.

94 M. J. Kleeman, J. J. Schauer and G. R. Cass, Size and Composition Distribution of Fine Particulate Matter Emitted from Wood Burning, Meat Charbroiling, and Cigarettes, *Environ. Sci. Technol.*, 1999, **33**(20), 3516–3523.

95 L. A. Garofalo, M. A. Pothier, E. J. T. Levin, T. Campos, S. M. Kreidenweis and D. K. Farmer, Emission and Evolution of Submicron Organic Aerosol in Smoke from Wildfires in the Western United States, *ACS Earth Space Chem.*, 2019, **3**(7), 1237–1247.

96 C. Samara, On the Redox Activity of Urban Aerosol Particles: Implications for Size Distribution and Relationships with Organic Aerosol Components, *Atmosphere*, 2017, **8**(10).

97 G. Simonetti, E. Conte, C. Perrino and S. Canepari, Oxidative potential of size-segregated PM in an urban and an industrial area of Italy, *Atmos. Environ.*, 2018, **187**, 292–300.

98 A. K. Cho, C. Sioutas, A. H. Miguel, Y. Kumagai, D. A. Schmitz, M. Singh, A. Eiguren-Fernandez and J. R. Froines, Redox activity of airborne particulate matter at different sites in the Los Angeles Basin, *Environ. Res.*, 2005, **99**(1), 40–47.

99 N. Li, M. Hao, R. F. Phalen, W. C. Hinds and A. E. Nel, Particulate air pollutants and asthma: A paradigm for the role of oxidative stress in PM-induced adverse health effects, *Clin. Immunol.*, 2003, **109**(3), 250–265.

100 M. Steenhof, I. Gosens, M. Strak, K. J. Godri, G. Hoek, F. R. Cassee, I. S. Mudway, F. J. Kelly, R. M. Harrison, E. Lebret, B. Brunekreef, N. A. H. Janssen and R. H. H. Pieters, In vitro toxicity of particulate matter (PM) collected at different sites in the Netherlands is associated with PM composition, size fraction and oxidative potential–the RAPTES project, *Part. Fibre Toxicol.*, 2011, **8**, 26.

101 J. G. Charrier, N. K. Richards-Henderson, K. J. Bein, A. S. McFall, A. S. Wexler and C. Anastasio, Oxidant production from source-oriented particulate matter - Part 1: Oxidative potential using the dithiothreitol (DTT) assay, *Atmos. Chem. Phys.*, 2015, **15**(5), 2327–2340.

102 T. Fang, L. Zeng, D. Gao, V. Verma, A. B. Stefaniak and R. J. Weber, Ambient Size Distributions and Lung Deposition of Aerosol Dithiothreitol-Measured Oxidative Potential: Contrast between Soluble and Insoluble Particles, *Environ. Sci. Technol.*, 2017, **51**(12), 6802–6811.

103 Z. H. Zhang, E. Hartner, B. Utinger, B. Gfeller, A. Paul, M. Sklorz, H. Czech, B. X. Yang, X. Y. Su, G. Jakobi, J. Orasche, J. Schnelle-Kreis, S. Jeong, T. Gröger, M. Pardo, T. Hohaus, T. Adam, A. Kiendler-Scharr, Y. Rudich, R. Zimmermann and M. Kalberer, Are reactive oxygen species (ROS) a suitable metric to predict toxicity of carbonaceous aerosol particles?, *Atmos. Chem. Phys.*, 2022, **22**(3), 1793–1809.

104 E. Chevallier, R. D. Jolibois, N. Meunier, P. Carlier and A. Monod, "Fenton-like" Reactions of Methylhydroperoxide and Ethylhydroperoxide with Fe 2+ in Liquid Aerosols under Tropospheric conditions, *Atmos. Environ.*, 2004, **38**(6), 921–933.

105 F. Leresche, J. R. Salazar, D. J. Pfotenhauer, M. P. Hannigan, B. J. Majestic and F. L. Rosario-Ortiz, Photochemical Aging of Atmospheric Particulate Matter in the Aqueous Phase, *Environ. Sci. Technol.*, 2021, **55**(19), 13152–13163.

106 S. Bogler, K. R. Daellenbach, D. M. Bell, A. S. H. Prévôt, I. El Haddad and N. Borduas-Dedekind, Singlet Oxygen Seasonality in Aqueous PM10 is Driven by Biomass Burning and Anthropogenic Secondary Organic Aerosol, *Environ. Sci. Technol.*, 2022, **56**(22), 15389–15397.

107 R. Kaur and C. Anastasio, First Measurements of Organic Triplet Excited States in Atmospheric Waters, *Environ. Sci. Technol.*, 2018, **52**(9), 5218–5226.

108 R. Kaur, J. R. Labins, S. S. Helbock, W. Jiang, K. J. Bein, Q. Zhang and C. Anastasio, Photooxidants from brown carbon and other chromophores in illuminated particle extracts, *Atmos. Chem. Phys.*, 2019, **19**(9), 6579–6594.

109 R. J. Yokelson, D. W. T. Griffith and D. E. Ward, Open-path Fourier transform infrared studies of large-scale laboratory biomass fires, *J. Geophys. Res.: Atmos.*, 1996, **101**(D15), 21067–21080.

110 A. Fushimi, K. Saitoh, K. Hayashi, K. Ono, Y. Fujitani, A. M. Villalobos, B. R. Shelton, A. Takami, K. Tanabe and J. J. Schauer, Chemical characterization and oxidative potential of particles emitted from open burning of cereal straws and rice husk under flaming and smoldering conditions, *Atmos. Environ.*, 2017, **163**, 118–127.